ELSEVIER

Journal of the Mechanics and Physics of Solids
52 (2004) 1719–1742

JOURNAL OF THE
MECHANICS AND
PHYSICS OF SOLIDS

www.elsevier.com/locate/jmps

# On ferroelectric crystals with engineered domain configurations

JiangYu Li*, Dan Liu

*Department of Engineering Mechanics, University of Nebraska-Lincoln, W317.5 Nebraska Hall, Lincoln, NE 68588-0526, USA*

Received 15 December 2003; received in revised form 16 February 2004; accepted 21 February 2004

**Abstract**

This paper examines the engineered domain configurations and the macroscopic properties of ferroelectric crystals using an energy minimization theory. The energy minimizing domain configurations have been constructed, and their macroscopic properties have been calculated and compared well with experiments. The optimal domain configurations have also been identified.


*Keywords:* Ferroelectrics; Engineered domain configurations; Energy minimization

## 1. Introduction

Domain configuration and its evolution under electromechanical loading is an outstanding problem in ferroelectrics that has attracted great research interest in the past decade. On the one hand, the evolution of domain configuration is responsible for the observed macroscopic nonlinearity in ferroelectrics, such as hysteresis loop and butterfly loop (Jona and Shirane, 1993); on the other hand, the complex nonlinear interactions between domains pose a significant challenge to the modelling and simulation of ferroelectrics. The problem is further complicated by the multiple length scales involved, ranging from domain walls, domains, grains, to ceramic inclusions in a composite. As a result, the macroscopic behaviors of ferroelectrics were traditionally modelled phenomenologically using energetic approaches without addressing the microstructural phenomena in details. Recently, micromechanics-informed phenomenological theories have been developed to include limited information at domain level, such as volume

* Corresponding author. Tel.: +1-402-472-1631; fax: +1-402-472-8292.
*E-mail address:* jiangyuli@unlnotes.unl.edu (J.Y. Li).

0022-5096/$ - see front matter © 2004 Elsevier Ltd. All rights reserved.
doi:10.1016/j.jmps.2004.02.011

fraction and shape of domains, but they often ignored the detailed structures of domains and domain walls (Hwang et al., 1995; Chen et al., 1997; Huber et al., 1999; Li and Weng, 1999). While those approaches have shed considerable insight on the macroscopic properties of ferroelectrics and are computationally inexpensive, they could not capture accurately the connection between macroscopic behaviors of ferroelectrics and their microstructural phenomena, which is still not well understood. Phase-field theory has also been developed to simulate the domain formation and domain pattern evolution in ferroelectrics (Nambu and Sagala, 1994; Hu and Chen, 1998; Li et al., 2001; Bhattacharya and Ravichandran, 2003), although they are computationally extensive and often limited to two-dimensional geometries. We hope to address these issues in this paper from a different perspective, i.e., constructing the detailed domain configurations analytically from the energy minimization. What we propose is a mesoscopic theory of ferroelectrics involving numerous domains, which collectively determine the macroscopic behavior of ferroelectrics. Despite tremendous progress made in the last decade in the quantum mechanical computations of ferroelectricity (Bellaiche et al., 2000; Fu and Cohen, 2000), the mesoscopic phenomena are currently beyond the capabilities of first principle calculations, and our mesoscopic approach is intended to fill this gap.

We are particularly interested in explaining the dramatically enhanced piezoelectricity in relaxor ferroelectric single crystals (Park and Shrout, 1997; Kuwata et al., 1982) using the engineered domain configurations, and in identifying the optimal domain configurations and poling directions for the optimized electromechanical couplings. The domain configurations in a ferroelectric arise from the minimization of its potential energy (Shu and Bhattacharya, 2001). When the crystal transforms from a nonpolar dielectric to a polar ferroelectric at Curie temperature, the reduction of symmetry leads to several symmetry-related, spontaneous polarized, and distorted variants, on which the stored energy density is minimized by the corresponding transformation strains and polarizations. Under a high electromechanical loading, a subset of ferroelectric variants will be selected which are energetically favored by the applied electromechanical field, leading to macroscopic piezoelectricity; this is the so-called poling. The selected variants need to be arranged in a compatible manner electromechanically to minimize their interaction energy, leading to complicated domain configurations, with the size of domains regulated by the domain wall energy. Having this energy minimization philosophy in mind, we seek to characterize the energy minimizing domain configurations in ferroelectrics and to predict their corresponding macroscopic properties. We will focus on the linear piezoelectricity of ferroelectrics without addressing the evolution of domain configurations. In other words, we assume that the domain configuration obtained by the poling is stable with the domain walls either pinned by defects or clamped within the domain configuration, and the applied electric field or mechanical stress during service is small and thus will not trigger domain switching. As such, we are dealing with the intrinsic piezoelectricity without concerning the extrinsic contribution from domain wall motions. This treatment is motivated by the enhanced piezoelectricity in relaxor crystals with engineered domain configurations, and we hope it can also help us to identify the optimal poling directions for the optimized electromechanical coupling. In addition, we feel that the understanding at the linear regime is essential for

our subsequent investigations on the domain evolution in ferroelectrics at higher electric field. Although our theory is developed for ferroelectrics, it can be easily adapted to other material systems involving phase transformations, such as shape memory alloys and ferromagnetic shape memory alloys.

As an application of the theory we will investigate the ultrahigh strain and piezoelectric behavior recently discovered in relaxor based rhombohedral single crystals $Pb(Mg_{1/3}Nb_{2/3})O_3$–$PbTiO_3$ (PMN–PT) and $Pb(Zn_{1/3}Nb_{2/3})O_3$–$PbTiO_3$ (PZN–PT) poled along the [0 0 1] direction (Park and Shrout, 1997; Kuwata et al., 1982), where the electromechanical coupling factor of more than 90% and piezoelectric strain of more than 1.5% were demonstrated. In contrast, PMN–PT and PZN–PT crystals poled along the [1 1 1] direction, the polar axis, exhibit much lower electromechanical coupling, and the question arises on the mechanism responsible for the dramatic piezoelectric property enhancement in these crystals. While it was suggested that the enhanced electromechanical coupling is related to the so-called engineered domain configuration, where two or more crystallographically equivalent ferroelectric variants coexist in a single crystal poled along a nonpolar axis (Park et al., 1999, Wada et al., 1999; Liu and Li, 2003), the exact nature of the enhancement and the optimal domain configuration are not clear, which we intend to address in this paper. We will carry out the detailed calculations on $BaTiO_3$ and PMN–PT to demonstrate that such engineered domain configurations indeed lead to enhanced piezoelectricity, and will identify the optimal domain configurations for the superior electromechanical coupling.

The paper is organized as follows. The energy minimization of ferroelectrics will be presented in Section 2, where the energetics of ferroelectrics will be discussed and energy minimizing domain configurations will be constructed. In Section 3, the equations for the effective electromechanical moduli of ferroelectrics with engineered domain configurations will be presented. The theory is then applied to tetragonal and rhombohedral crystals poled along a nonpolar axis, and compared with available experimental data. Optimal electromechanical poling and domain configurations will also be identified.

## 2. Energy minimization of ferroelectrics

In this section, we seek to characterize ferroelectric single crystals with engineered domain configuration. The energetics of ferroelectrics will be given first, and the energy minimizing domain configuration will then be constructed using multi-rank laminates.

### 2.1. Energetics of ferroelectrics

We consider a ferroelectric/conductor system, where $\Omega \in \mathbb{R}^3$ is a bounded domain occupied by a ferroelectric subject to an applied traction $\mathbf{T}_0$ on $\partial\Omega_2$, and $C_1$ and $C_2$ are domains occupied by conductors with total charge $Q$ and fixed potential $\phi^0$, respectively. In addition, we assume the ferroelectric experiences a deformation $\mathbf{u}(\mathbf{x}) : \Omega \to \mathbb{R}^3$ and a polarization $\mathbf{p}(\mathbf{x}) : \Omega \to \mathbb{R}^3$ due to the applied electromechanical load.

Under the infinitesimal strain approximation, the potential energy of the ferroelectric is given by (Shu and Bhattacharya, 2001)

$$F(\mathbf{u},\mathbf{p}) = \int_{\Omega} \left( \frac{1}{2} \nabla \mathbf{p} \cdot \mathbf{a} \nabla \mathbf{p} + W(\mathbf{e}[\mathbf{u}],\mathbf{p}) - \mathbf{E}_0 \cdot \mathbf{p} \right) \mathrm{d}\mathbf{x} - \int_{\partial\Omega_2} \mathbf{T}_0 \cdot \mathbf{u} \mathrm{d}S + \frac{\varepsilon_0}{2} \int_{\mathbb{R}^3} |\nabla \phi|^2 \, \mathrm{d}\mathbf{x}, \tag{2.1}$$

where $\mathbf{e}[\mathbf{u}] = \frac{1}{2}(\nabla \mathbf{u} + (\nabla \mathbf{u})^{\mathrm{t}})$ is the symmetric infinitesimal strain tensor and $\phi$ is the electric potential, obtained by solving Maxwell's equation in $\mathbb{R}^3$,

$$\nabla \cdot (-\varepsilon_0 \nabla \phi + \mathbf{p}\chi_{\Omega}) = \nabla \cdot \mathbf{D} = \rho_{\mathrm{f}}, \tag{2.2}$$

subjected to the boundary conditions

$$\begin{aligned} &\int_{\partial C_1} \frac{\partial \phi}{\partial n} \mathrm{d}S = 0, \quad \nabla \phi = \mathbf{0} \quad \text{on } C_1, \\ &\phi = 0 \quad \text{on } C_2, \\ &\phi \to 0 \text{ as } |\mathbf{x}| \to \infty, \end{aligned} \tag{2.3}$$

where

$$\chi_{\Omega}(\mathbf{x}) = \begin{cases} 1 & \text{if} \quad \mathbf{x} \in \Omega, \\ 0 & \text{if} \quad \mathbf{x} \in \mathbb{R}^3 \setminus \Omega \end{cases}$$

is the characteristic function of $\Omega$, $\mathbf{0}$ is the null vector, $\mathbf{D}$ is the electric displacement, and $\rho_{\mathrm{f}}$ is the free charge density which is assumed to be zero in the ferroelectric; as such $\mathbf{D}$ is divergence-free except on the surface of conductors. $\mathbf{E}_0$ is the electric field in the absence of the ferroelectric, which is determined by solving

$$-\varepsilon_0 \nabla^2 \phi_0 = \rho_{\mathrm{f}_0} \tag{2.4}$$

for $\phi_0$ subjected to

$$\begin{aligned} &\int_{\partial C_1} \frac{\partial \phi_0}{\partial n} \mathrm{d}S = -\frac{Q}{\varepsilon_0}, \ \nabla \phi_0 = \mathbf{0} \quad \text{on } C_1, \\ &\phi_0 = \phi^0 \quad \text{on } C_2, \\ &\phi_0 \to 0 \text{ as } |\mathbf{x}| \to \infty, \end{aligned} \tag{2.5}$$

where all variables with a subscript 0 denote the quantities in the absence of the ferroelectric.

In the potential energy (2.1), the second term is the 'stored energy density' of the ferroelectric which depends on the state variables, strain $\mathbf{e}[\mathbf{u}]$ and polarization $\mathbf{p}$. It encodes the information that the ferroelectric prefers certain states of transformation strain and polarization. In particular, it has a multi-well structure, leading to 'variants' or 'domains' of different transformation strains and polarizations separated by

'domain walls'. The domain wall energy is represented by the first term of the potential energy which penalizes the polarization gradient, where **a** is a positive definite second order tensor. The third term is the potential associated with the applied electric field $\mathbf{E}_0$ which tends to align the polarization towards $\mathbf{E}_0$, and the fourth term is the energy associated with the applied mechanical load. The final term is the depolarization energy due to the electric field generated by the polarization distribution in the ferroelectric, where $\varepsilon_0 = 8.85 \times 10^{-12}$ C$^2$/Nm$^2$ is the permittivity of free space.

This type of potential energy is justified in Shu and Bhattacharya (2001) following ideas in micromagnetics (Brown, 1963; James and Kinderlehrer, 1993), by considering the total energy of the ferroelectric-conductor system described and excluding the energy of the conductors in the absence of the ferroelectric. Detailed derivation can be found in Shu and Bhattacharya (2001) and will not be repeated here. However, we do want to emphasize the difference between ferroelectrics and shape memory alloys or ferromagnetics here. For shape memory alloy, there is no energy term analog to the depolarization energy, while for ferromagnetics, the anisotropy energy is usually comparable in magnitude to Zeeman's energy caused by the applied magnetic field, and is not nearly as dominating as the stored energy density in ferroelectrics. These differences will lead to subtle differences in domain configurations, as we will elaborate later.

### 2.2. Energy-minimizing domain configurations

We are interested in the equilibrium domain configurations in ferroelectrics under electromechanical loadings, and propose that such domain configurations minimize the potential energy (2.1). In order to construct the domain configuration in an energy minimizing manner, we consider a constrained theory of ferroelectrics, which is adapted from the constrained theory of magnetoelastic solids (DeSimone and James, 2002). In particular, we assume that the transformation strain **e** and polarization **p** of a ferroelectric are constrained within the multiple energy wells $\mathscr{K}$,

$$(\mathbf{e}, \mathbf{p}) \in \mathscr{K} = \bigcup_{i=1}^{K} \{(\mathbf{e}^{(i)}, \mathbf{p}^{(i)})\},$$

which contains $K$ energy wells or variants with transformation strain $\mathbf{e}^{(i)}$ and polarization $\mathbf{p}^{(i)}$. As a result, we have

$$W(\mathbf{e}, \mathbf{p}) = 0.$$

In addition, we assume the size of the ferroelectric domain is much larger than the domain wall thickness, so that the domain wall energy can be ignored (DeSimone, 1993). The electromechanical loading, $\mathbf{T}_0$ and $\mathbf{E}_0$, will then select a subset of ferroelectric variants from $\mathscr{K}$ which are energetically favored. As a result, we only need to minimize the depolarization energy by arranging polarization distribution, or the selected ferroelectric variants, in an energy minimizing manner. To this end, we must consider the compatibility between ferroelectric variants.

One pair of ferroelectric variants $(\mathbf{e}^{(1)}, \mathbf{p}^{(1)})$ and $(\mathbf{e}^{(2)}, \mathbf{p}^{(2)})$ are said to be compatible if they satisfy

$$\mathbf{e}^{(1)} - \mathbf{e}^{(2)} = \tfrac{1}{2}(\mathbf{a} \otimes \mathbf{n} + \mathbf{n} \otimes \mathbf{a}),$$
$$(\mathbf{p}^{(1)} - \mathbf{p}^{(2)}) \cdot \mathbf{n} = 0 \tag{2.6}$$

for some unit vector $\mathbf{n}$ and vector $\mathbf{a}$. Here we do not differentiate polarization in the deformed and nondeformed configurations, since the strain is assumed to be small. $(2.6)_1$ is the Hadamard jump condition that ensures the existence of a nontrivial continuous displacement field $\mathbf{u}$ across a coherent interface with normal $\mathbf{n}$ such that $[(\nabla\mathbf{u} + \nabla\mathbf{u}^{\mathrm{T}})/2] \in \{\mathbf{e}^{(1)}, \mathbf{e}^{(2)}\}$, and $(2.6)_2$ ensures that $\mathbf{p} \in \{\mathbf{p}^{(1)}, \mathbf{p}^{(2)}\}$ is divergence free with interface normal $\mathbf{n}$, and thus cost no extra depolarization energy. As a result, an energy-minimizing rank-one laminate can be formed consisting of variants 1 and 2 with interface normal given by $\mathbf{n}$.

For a more general case with $K$ ferroelectric variants, the set $\mathscr{K}$ is said to consist of $K$ pair-wise compatible ferroelectric variants if there exist vectors $\mathbf{n}_{jk}$ and $\mathbf{a}_{jk}$, where $j, k = 1, \ldots K$, such that

$$\mathbf{e}^{(j)} - \mathbf{e}^{(k)} = \tfrac{1}{2}(\mathbf{a}_{jk} \otimes \mathbf{n}_{jk} + \mathbf{n}_{jk} \otimes \mathbf{a}_{jk}),$$
$$(\mathbf{p}^{(j)} - \mathbf{p}^{(k)}) \cdot \mathbf{n}_{jk} = 0. \tag{2.7}$$

If (2.7) is satisfied, then the $K$ variants can still form an energy minimizing domain configuration by arbitrary volume fractions, which can be constructed by multi-rank laminates. The following construction is in analog to DeSimone and James' construction in magnetoelasticity (2002), extending Bhattacharya's work in martensitic transformation (1993). We repeat the construction here since it is essential for the understanding of our subsequent analysis.

To this end we consider a set of variants coexisting in a ferroelectric crystal, with transformation strain and polarization satisfying (2.7); the volume fraction of each variant is $\lambda_i$, which could be determined by the applied electromechanical loading. The average strain $\langle\mathbf{e}\rangle$ and polarization $\langle\mathbf{p}\rangle$ of the ferroelectric crystal are thus given by

$$\langle\mathbf{e}\rangle = \sum_{i=1}^{K} \lambda_i \mathbf{e}^{(i)}, \quad \langle\mathbf{p}\rangle = \sum_{i=1}^{K} \lambda_i \mathbf{p}^{(i)}, \quad \text{where } \lambda_i \geqslant 0, \quad \sum_{i=1}^{K} \lambda_i = 1, \tag{2.8}$$

and we seek to construct an energy minimizing domain configuration satisfying (2.8). As a matter of fact, given (2.7) and any $\mu_1, \ldots, \mu_{K-1} \in [0, 1]$, it is possible to form an energy minimizing domain configuration such that

$$\langle\mathbf{e}\rangle = \mu_1\mathbf{e}^{(1)} + \mu_2(1-\mu_1)\mathbf{e}^{(2)} + \cdots + \mu_{K-1}\prod_{r=1}^{K-2}(1-\mu_r)\mathbf{e}^{(K-1)} + \prod_{r-1}^{K-1}(1-\mu_r)\mathbf{e}^{(K)},$$

$$\langle\mathbf{p}\rangle = \mu_1\mathbf{p}^{(1)} + \mu_2(1-\mu_1)\mathbf{p}^{(2)} + \cdots + \mu_{K-1}\prod_{r=1}^{K-2}(1-\mu_r)\mathbf{p}^{(K-1)} + \prod_{r-1}^{K-1}(1-\mu_r)\mathbf{p}^{(K)},$$

which can be proven by induction. We will show the case $K=3$ explicitly to illustrate the method. By (2.7), we have

$$\mathbf{e}^{(1)}-\mathbf{e}^{(2)}=\tfrac{1}{2}(\mathbf{a}_{12}\otimes\mathbf{n}_{12}+\mathbf{n}_{12}\otimes\mathbf{a}_{12}),$$

$$\mathbf{e}^{(1)}-\mathbf{e}^{(3)}=\tfrac{1}{2}(\mathbf{a}_{13}\otimes\mathbf{n}_{13}+\mathbf{n}_{13}\otimes\mathbf{a}_{13}),$$

$$\mathbf{e}^{(2)}-\mathbf{e}^{(3)}=\tfrac{1}{2}(\mathbf{a}_{23}\otimes\mathbf{n}_{23}+\mathbf{n}_{23}\otimes\mathbf{a}_{23}), \tag{2.9}$$

and

$$(\mathbf{p}^{(1)}-\mathbf{p}^{(2)})\cdot\mathbf{n}_{12}=0,$$

$$(\mathbf{p}^{(1)}-\mathbf{p}^{(3)})\cdot\mathbf{n}_{13}=0,$$

$$(\mathbf{p}^{(2)}-\mathbf{p}^{(3)})\cdot\mathbf{n}_{23}=0. \tag{2.10}$$

Thus, for any $\mu_1\in[0,1]$, we have

$$(\mu_1\mathbf{e}^{(1)}+(1-\mu_1)\mathbf{e}^{(2)})-(\mu_1\mathbf{e}^{(1)}+(1-\mu_1)\mathbf{e}^{(3)})=\frac{1-\mu_1}{2}(\mathbf{a}_{23}\otimes\mathbf{n}_{23}+\mathbf{n}_{23}\otimes\mathbf{a}_{23})$$

and

$$((\mu_1\mathbf{p}^{(1)}+(1-\mu_1)\mathbf{p}^{(2)})-(\mu_1\mathbf{p}^{(1)}+(1-\mu_1)\mathbf{p}^{(3)}))\cdot\mathbf{n}_{23}=0. \tag{2.11}$$

Now find skew matrices $\mathbf{w}_1$, $\mathbf{w}_2$, $\mathbf{w}_3$, $\mathbf{w}_4$ that satisfy

$$\mathbf{w}_1-\mathbf{w}_2=\tfrac{1}{2}(\mathbf{a}_{12}\otimes\mathbf{n}_{12}-\mathbf{n}_{12}\otimes\mathbf{a}_{12})\equiv\mathbf{v}_1,$$

$$\mathbf{w}_3-\mathbf{w}_4=\tfrac{1}{2}(\mathbf{a}_{13}\otimes\mathbf{n}_{13}-\mathbf{n}_{13}\otimes\mathbf{a}_{13})\equiv\mathbf{v}_2,$$

$$(\mu_1\mathbf{w}_1+(1-\mu_1)\mathbf{w}_2)-(\mu_1\mathbf{w}_3+(1-\mu_1)\mathbf{w}_4)=\frac{1-\mu_1}{2}(\mathbf{a}_{23}\otimes\mathbf{n}_{23}-\mathbf{n}_{23}\otimes\mathbf{a}_{23})\equiv\mathbf{v}_3,$$

$$\mu_2(\mu_1\mathbf{w}_1+(1-\mu_1)\mathbf{w}_2)+(1-\mu_2)(\mu_1\mathbf{w}_3+(1-\mu_1)\mathbf{w}_4)=0. \tag{2.12}$$

It is easy to verify that

$$\mathbf{w}_1=(1-\mu_1)\mathbf{v}_1+(1-\mu_2)\mathbf{v}_3,$$

$$\mathbf{w}_2=-\mu_1\mathbf{v}_1+(1-\mu_2)\mathbf{v}_3,$$

$$\mathbf{w}_3=(1-\mu_1)\mathbf{v}_2-\mu_2\mathbf{v}_3,$$

$$\mathbf{w}_4=-\mu_1\mathbf{v}_2-\mu_2\mathbf{v}_3 \tag{2.13}$$

satisfy (2.12). Now let us set

$$\mathbf{F}_1=\mathbf{e}^{(1)}+\mathbf{w}_1+\mathbf{i}_2,$$

$$\mathbf{F}_2=\mathbf{e}^{(2)}+\mathbf{w}_2+\mathbf{i}_2,$$

$$\mathbf{F}_3=\mathbf{e}^{(1)}+\mathbf{w}_3+\mathbf{i}_2,$$

$$\mathbf{F}_4=\mathbf{e}^{(3)}+\mathbf{w}_4+\mathbf{i}_2, \tag{2.14}$$

where $\mathbf{i}_2$ is the second rank unit tensor. Clearly, $\mathbf{F}_i$ are contained in the energy wells. They also satisfy

$$\mathbf{F}_1 - \mathbf{F}_2 = \mathbf{a}_{12} \otimes \mathbf{n}_{12},$$

$$\mathbf{F}_3 - \mathbf{F}_4 = \mathbf{a}_{13} \otimes \mathbf{n}_{13},$$

$$(\mu_1\mathbf{F}_1 + (1-\mu_1)\mathbf{F}_2) - (\mu_1\mathbf{F}_3 + (1-\mu_1)\mathbf{F}_4) = (1-\mu_1)\mathbf{a}_{23} \otimes \mathbf{n}_{23}. \tag{2.15}$$

Therefore, it is possible to construct the sequence of deformation made of alternating bands of fine twins of $(\mathbf{F}_1, \mathbf{p}^{(1)})$ and $(\mathbf{F}_2, \mathbf{p}^{(2)})$, and fine twins of $(\mathbf{F}_3, \mathbf{p}^{(1)})$ and $(\mathbf{F}_4, \mathbf{p}^{(3)})$ (Ball and James, 1992; Bhattacharya, 1993; DeSimone and James, 2002), with the average strain and polarization given by

$$\langle \mathbf{e} \rangle = \mu_1\mathbf{e}^{(1)} + (1-\mu_1)\mu_2\mathbf{e}^{(2)} + (1-\mu_1)(1-\mu_2)\mathbf{e}^{(3)},$$

$$\langle \mathbf{p} \rangle = \mu_1\mathbf{p}^{(1)} + (1-\mu_1)\mu_2\mathbf{p}^{(2)} + (1-\mu_1)(1-\mu_2)\mathbf{p}^{(3)}. \tag{2.16}$$

No depolarization energy is induced since (2.11) is satisfied. This completes the proof for $K = 3$.

Now, suppose, it holds for the case $K = n$, and we show that it also holds for $K = n + 1$. Picking $n$ pairs of $(\mathbf{e}^{(1)}, \mathbf{p}^{(1)}), (\mathbf{e}^{(2)}, \mathbf{p}^{(2)}), \ldots, (\mathbf{e}^{(n-1)}, \mathbf{p}^{(n-1)})$ and $(\mathbf{e}^{(n)}, \mathbf{p}^{(n)})$, and by hypothesis we can form a domain configuration with

$$\mathbf{e}^{\mathrm{I}} = \mu_1\mathbf{e}^{(1)} + \mu_2(1-\mu_1)\mathbf{e}^{(2)} + \cdots + \mu_{n-1}\prod_{r=1}^{n-2}(1-\mu_r)\mathbf{e}^{(n-1)} + \prod_{r-1}^{n-1}(1-\mu_r)\mathbf{e}^{(n)},$$

$$\mathbf{p}^{\mathrm{I}} = \mu_1\mathbf{p}^{(1)} + \mu_2(1-\mu_1)\mathbf{p}^{(2)} + \cdots + \mu_{n-1}\prod_{r=1}^{n-2}(1-\mu_r)\mathbf{p}^{(n-1)} + \prod_{r-1}^{n-1}(1-\mu_r)\mathbf{p}^{(n)}.$$

Picking another $n$ pairs of $(\mathbf{e}^{(1)}, \mathbf{p}^{(1)}), (\mathbf{e}^{(2)}, \mathbf{p}^{(2)}), \ldots, (\mathbf{e}^{(n-1)}, \mathbf{p}^{(n-1)})$ and $(\mathbf{e}^{(n+1)}, \mathbf{p}^{(n+1)})$, and by hypothesis we can form another domain configuration with

$$\mathbf{e}^{\mathrm{II}} = \mu_1\mathbf{e}^{(1)} + \mu_2(1-\mu_1)\mathbf{e}^{(2)} + \cdots + \mu_{n-1}\prod_{r=1}^{n-2}(1-\mu_r)\mathbf{e}^{(n-1)} + \prod_{r-1}^{n-1}(1-\mu_r)\mathbf{e}^{(n+1)},$$

$$\mathbf{p}^{\mathrm{II}} = \mu_1\mathbf{p}^{(1)} + \mu_2(1-\mu_1)\mathbf{p}^{(2)} + \cdots + \mu_{n-1}\prod_{r=1}^{n-2}(1-\mu_r)\mathbf{p}^{(n-1)} + \prod_{r-1}^{n-1}(1-\mu_r)\mathbf{p}^{(n+1)}.$$

Notice that

$$\mathbf{e}^{\mathrm{I}} - \mathbf{e}^{\mathrm{II}} = \frac{1}{2}\prod_{r=1}^{n-1}(1-\mu_r)(\mathbf{a}_{n(n+1)} \otimes \mathbf{n}_{n(n+1)} - \mathbf{n}_{n(n+1)} \otimes \mathbf{a}_{n(n+1)}),$$

$$(\mathbf{p}^{\mathrm{I}} - \mathbf{p}^{\mathrm{II}}) \cdot \mathbf{n}_{n(n+1)} = \prod_{r=1}^{n-1}(1-\mu_r)(\mathbf{p}^{(n)} - \mathbf{p}^{(n+1)}) \cdot \mathbf{n}_{n(n+1)} = 0,$$

thus by hypothesis, it is possible to form a laminate consisting of alternating bands of $(\mathbf{e}^{\mathrm{I}}, \mathbf{p}^{\mathrm{I}})$ and $(\mathbf{e}^{\mathrm{II}}, \mathbf{p}^{\mathrm{II}})$, with the average strain and polarization given by

$$\langle \mathbf{e} \rangle = \mu_n \mathbf{e}^{\mathrm{I}} + (1-\mu_n)\mathbf{e}^{\mathrm{II}},$$
$$\langle \mathbf{p} \rangle = \mu_n \mathbf{p}^{\mathrm{I}} + (1-\mu_n)\mathbf{p}^{\mathrm{II}}, \tag{2.17}$$

for any $\mu_n \in [0,1]$. This completes the proof.

It remains to show that given any $\{\lambda_r : \lambda_r \geqslant 0, \sum_{r=1}^{K} \lambda_r = 1\}$, we can find $\mu_r \in [0,1]$, $r = 1, \ldots K$, such that

$$\lambda_r = \begin{cases} \mu_r \displaystyle\prod_{i=1}^{r-1}(1-\mu_i), & r = 1, \ldots K-1, \\ \displaystyle\prod_{i=1}^{r-1}(1-\mu_i), & r = K. \end{cases} \tag{2.18}$$

This is true for the following choice of $\mu_r$ (Bhattacharya, 1993),

$$\mu_r = \begin{cases} 0, & \displaystyle\sum_{i=1}^{r-1} \lambda_i = 1, \\ \dfrac{\lambda_r}{1 - \sum_{i=1}^{r-1} \lambda_i} & \text{otherwise.} \end{cases} \tag{2.19}$$

As a result, it is possible to construct an energy minimizing domain configuration using multi-rank laminates when the ferroelectric variants are pair-wise compatible.

## 3. The effective moduli of ferroelectric crystals

With the energy minimizing domain configuration of a ferroelectric crystal constructed by the multi-rank lamination, we seek to determine its linear electromechanical behavior under a small applied field. Laminated materials have been analyzed extensively for the effective conductivity, elasticity, and thermoelasticity, and a comprehensive review can be found in Milton (2002). Here, we assume that the applied field under consideration is not large enough to trigger domain switching, so that the linear piezoelectric theory applies, with the static piezoelectric constitutive equation given by

$$\begin{bmatrix} e_1 \\ e_2 \\ e_3 \\ e_4 \\ e_5 \\ e_6 \\ D_1 \\ D_2 \\ D_3 \end{bmatrix} = \begin{bmatrix} S_{11} & S_{12} & S_{13} & S_{14} & S_{15} & S_{16} & d_{11} & d_{21} & d_{31} \\ S_{12} & S_{22} & S_{23} & S_{24} & S_{25} & S_{26} & d_{12} & d_{22} & d_{32} \\ S_{13} & S_{23} & S_{33} & S_{34} & S_{35} & S_{36} & d_{13} & d_{23} & d_{33} \\ S_{14} & S_{24} & S_{34} & S_{44} & S_{45} & S_{46} & d_{14} & d_{24} & d_{34} \\ S_{15} & S_{25} & S_{35} & S_{45} & S_{55} & S_{56} & d_{15} & d_{25} & d_{35} \\ S_{16} & S_{26} & S_{36} & S_{46} & S_{56} & S_{66} & d_{16} & d_{26} & d_{36} \\ d_{11} & d_{12} & d_{13} & d_{14} & d_{15} & d_{16} & \kappa_{11} & \kappa_{12} & \kappa_{13} \\ d_{21} & d_{22} & d_{23} & d_{24} & d_{25} & d_{26} & \kappa_{12} & \kappa_{22} & \kappa_{23} \\ d_{31} & d_{32} & d_{33} & d_{34} & d_{35} & d_{36} & \kappa_{13} & \kappa_{23} & \kappa_{33} \end{bmatrix} \begin{bmatrix} \sigma_1 \\ \sigma_2 \\ \sigma_3 \\ \sigma_4 \\ \sigma_5 \\ \sigma_6 \\ E_1 \\ E_2 \\ E_3 \end{bmatrix}, \tag{3.1}$$

which can be rearranged as

$$\begin{bmatrix} \mathbf{Y} \\ \mathbf{Z} \end{bmatrix} = \begin{bmatrix} \mathbf{A} & \mathbf{B} \\ \mathbf{B}^{\mathrm{t}} & \mathbf{N} \end{bmatrix} \begin{bmatrix} \mathbf{F} \\ \mathbf{G} \end{bmatrix}, \tag{3.2}$$

where superscript t is used to denote a matrix transpose, and the field variables and the electromechanical moduli are given by

$$\mathbf{Y} = \begin{bmatrix} e_1 \\ e_2 \\ e_6 \\ D_3 \end{bmatrix}, \quad \mathbf{Z} = \begin{bmatrix} e_3 \\ e_4 \\ e_5 \\ D_1 \\ D_2 \end{bmatrix}, \quad \mathbf{F} = \begin{bmatrix} \sigma_1 \\ \sigma_2 \\ \sigma_6 \\ E_3 \end{bmatrix}, \quad \mathbf{G} = \begin{bmatrix} \sigma_3 \\ \sigma_4 \\ \sigma_5 \\ E_1 \\ E_2 \end{bmatrix},$$

and

$$\mathbf{A} = \begin{bmatrix} S_{11} & S_{12} & S_{16} & d_{31} \\ S_{12} & S_{22} & S_{26} & d_{32} \\ S_{16} & S_{26} & S_{66} & d_{36} \\ d_{31} & d_{32} & d_{36} & \kappa_{33} \end{bmatrix},$$

$$\mathbf{B} = \begin{bmatrix} S_{13} & S_{14} & S_{15} & d_{11} & d_{21} \\ S_{23} & S_{24} & S_{25} & d_{12} & d_{22} \\ S_{36} & S_{46} & S_{56} & d_{16} & d_{26} \\ d_{33} & d_{34} & d_{35} & \kappa_{13} & \kappa_{23} \end{bmatrix},$$

$$\mathbf{N} = \begin{bmatrix} S_{33} & S_{34} & S_{35} & d_{13} & d_{23} \\ S_{34} & S_{44} & S_{45} & d_{14} & d_{24} \\ S_{35} & S_{45} & S_{55} & d_{15} & d_{25} \\ d_{13} & d_{14} & d_{15} & \kappa_{11} & \kappa_{12} \\ d_{23} & d_{24} & d_{25} & \kappa_{12} & \kappa_{22} \end{bmatrix}.$$

Now, let us consider the linear piezoelectric behavior of a ferroelectric laminate consisting of two variants as shown in Fig. 1. Notice that the normal of the laminate is chosen as the $x_3$ axis, which allows us to take advantage of electromechanical continuity conditions at the interface. For each variant $r=1,2$, the constitutive equations are given by

$$\begin{bmatrix} \mathbf{Y}_r \\ \mathbf{Z}_r \end{bmatrix} = \begin{bmatrix} \mathbf{A}_r & \mathbf{B}_r \\ \mathbf{B}_r^{\mathrm{t}} & \mathbf{N}_r \end{bmatrix} \begin{bmatrix} \mathbf{F}_r \\ \mathbf{G}_r \end{bmatrix}, \tag{3.3}$$

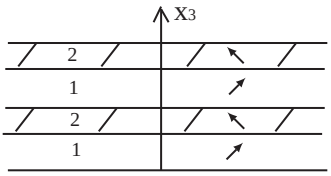


Fig. 1. A ferroelectric laminate consisting of two variants.

leading to a heterogeneous electromechanical field distribution in the laminate. The continuity conditions at the interface, however, require that

$$\mathbf{Y}_1 = \mathbf{Y}_2 = \bar{\mathbf{Y}}, \quad \mathbf{G}_1 = \mathbf{G}_2 = \bar{\mathbf{G}}, \tag{3.4}$$

where the overhead bar is used to denote volume averaged field variables in the laminate. As a result, for each phase we have

$$\begin{aligned} \mathbf{F}_r &= \mathbf{A}_r^{-1}\bar{\mathbf{Y}} - \mathbf{A}_r^{-1}\mathbf{B}_r\bar{\mathbf{G}}, \\ \mathbf{Z}_r &= \mathbf{B}_r^{\mathrm{t}}\mathbf{F}_r + \mathbf{N}_r\bar{\mathbf{G}} = \mathbf{B}_r^{\mathrm{t}}\mathbf{A}_r^{-1}\bar{\mathbf{Y}} + (\mathbf{N}_r - \mathbf{B}_r^{\mathrm{t}}\mathbf{A}_r^{-1}\mathbf{B}_r)\bar{\mathbf{G}}, \end{aligned} \tag{3.5}$$

where subscript $r$ is used to denote a field variable in phase $r$, which leads to

$$\begin{aligned} \bar{\mathbf{F}} &= \langle \mathbf{A}^{-1}\rangle\bar{\mathbf{Y}} - \langle \mathbf{A}^{-1}\mathbf{B}\rangle\bar{\mathbf{G}}, \\ \bar{\mathbf{Z}} &= \langle \mathbf{B}^{\mathrm{t}}\mathbf{A}^{-1}\rangle\bar{\mathbf{Y}} + (\langle \mathbf{N}\rangle - \langle \mathbf{B}^{\mathrm{t}}\mathbf{A}^{-1}\mathbf{B}\rangle)\bar{\mathbf{G}}, \end{aligned} \tag{3.6}$$

where $\langle\cdot\rangle$ is used to denote volume averaged physical properties. Rearranging the equations yields

$$\begin{aligned} \bar{\mathbf{Y}} &= \langle \mathbf{A}^{-1}\rangle^{-1}\bar{\mathbf{F}} + \langle \mathbf{A}^{-1}\rangle^{-1}\langle \mathbf{A}^{-1}\mathbf{B}\rangle\bar{\mathbf{G}}, \\ \bar{\mathbf{Z}} &= \langle \mathbf{B}^{\mathrm{t}}\mathbf{A}^{-1}\rangle\langle \mathbf{A}^{-1}\rangle^{-1}\bar{\mathbf{F}} + (\langle \mathbf{B}^{\mathrm{t}}\mathbf{A}^{-1}\rangle\langle \mathbf{A}^{-1}\rangle^{-1}\langle \mathbf{A}^{-1}\mathbf{B}\rangle \\ &\quad + \langle \mathbf{N}\rangle - \langle \mathbf{B}^{\mathrm{t}}\mathbf{A}^{-1}\mathbf{B}\rangle)\bar{\mathbf{G}}, \end{aligned} \tag{3.7}$$

which leads to the following effective electromechanical moduli:

$$\begin{aligned} \mathbf{A}^* &= \langle \mathbf{A}^{-1}\rangle^{-1}, \\ \mathbf{B}^* &= \langle \mathbf{A}^{-1}\rangle^{-1}\langle \mathbf{A}^{-1}\mathbf{B}\rangle, \\ \mathbf{B}^{\mathrm{t}^*} &= \langle \mathbf{B}^{\mathrm{t}}\mathbf{A}^{-1}\rangle\langle \mathbf{A}^{-1}\rangle^{-1}, \\ \mathbf{N}^* &= \langle \mathbf{B}^{\mathrm{t}}\mathbf{A}^{-1}\rangle\langle \mathbf{A}^{-1}\rangle^{-1}\langle \mathbf{A}^{-1}\mathbf{B}\rangle + \langle \mathbf{N}\rangle - \langle \mathbf{B}^{\mathrm{t}}\mathbf{A}^{-1}\mathbf{B}\rangle. \end{aligned} \tag{3.8}$$

Clearly, the matrix of the effective electromechanical moduli is diagonally symmetric. Eqs. (3.8) are exact for rank-one laminates, but can also be applied to calculate the effective electromechanical moduli of a multi-rank laminate if there is separation of scales between different levels, so that the lower level laminates can be regarded as homogeneous as far as the effective behavior of higher level laminate is concerned. They are explicit algebraic equations that can be numerically implemented easily. As such, we

can use it to determine the electromechanical behavior of ferroelectric single crystals with engineered domain configurations. Combining with appropriate micromechanics approximation, it can also be applied to study the effective properties of ferroelectric ceramics (Dunn, 1995; Li, 2000).

## 4. Ferroelectric crystals with engineered domain configurations

We now apply the theory to ferroelectrics with engineered domain configurations, including tetragonal crystal such as $BaTiO_3$ and rhombohedral crystal such as PMN–PT.

### 4.1. Tetragonal crystal

We first consider a tetragonal crystal, where the transformation strains and polarizations are given by

$$\mathbf{e}^{(\pm1)} = \begin{bmatrix} \beta & 0 & 0 \\ 0 & \alpha & 0 \\ 0 & 0 & \alpha \end{bmatrix}, \quad \mathbf{p}^{(\pm1)} = \pm \begin{bmatrix} p_t \\ 0 \\ 0 \end{bmatrix},$$

$$\mathbf{e}^{(\pm2)} = \begin{bmatrix} \alpha & 0 & 0 \\ 0 & \beta & 0 \\ 0 & 0 & \alpha \end{bmatrix}, \quad \mathbf{p}^{(\pm2)} = \pm \begin{bmatrix} 0 \\ p_t \\ 0 \end{bmatrix},$$

$$\mathbf{e}^{(\pm3)} = \begin{bmatrix} \alpha & 0 & 0 \\ 0 & \alpha & 0 \\ 0 & 0 & \beta \end{bmatrix}, \quad \mathbf{p}^{(\pm3)} = \pm \begin{bmatrix} 0 \\ 0 \\ p_t \end{bmatrix} \tag{4.1}$$

with respect to the cubic crystallographic axes. There are in total six ferroelectric variants, with variants $\pm i$ having opposite polarization directions yet identical transformation strain. It can be easily verified that each pair of variants is compatible, satisfying (2.7).

If such a tetragonal crystal is poled by an electric field along the [1 1 1] axis,

$$\mathbf{E}_0 = [1,1,1]E_0 \quad \text{and} \quad \mathbf{T}_0 = \mathbf{0},$$

as shown in Fig. 2, then three variants 1, 2, and 3 with positive polarization component will coexist in ferroelectric to minimize the potential energy with the electric field, since variants $-1$, $-2$, and $-3$ are energetically disfavored. In addition, they will have equal volume fraction, $\lambda_i = \frac{1}{3}$, to minimize the depolarization energy. Otherwise, the crystal will have net polarization component parallel to the (1 1 1) planes which are deposited with electrode, leading to nonzero depolarization field. It is worthwhile to comment on similar situations in shape memory alloys and ferromagnetics. If an external stress is applied to a tetragonal shape memory alloy along the [1 1 1] axis,

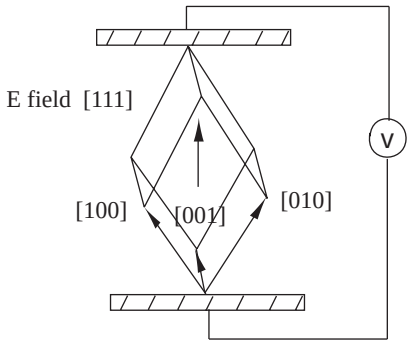


Fig. 2. The coexistence of three ferroelectric variants in the [1 1 1] poled tetragonal crystal.

three variants will coexist. However, if the stress is slightly deviated from the [1 1 1] axis, only one variant favored by the deviated stress will exist. This will not occur in ferroelectrics if the applied electric field is slightly deviated from the [1 1 1] axis thanks to the influence of depolarization energy. On the other hand, if a magnetic field along the [1 1 1] axis is applied to a ferromagnetic with the easy axes along $\langle 1\,0\,0\rangle$, the magnetization will gradually rotate from the easy axis to the [1 1 1] axis, resulting in a uniform magnetization after saturation. This again, will not occur in ferroelectrics, since anisotropy energy, or the stored energy density, is much stronger in ferroelectrics than in ferromagnetics compared to the energy caused by the external field, and polarization rotation will not occur under an ordinary electric field. If an extremely high electric field is applied to a tetragonal ferroelectric along the [1 1 1] axis, then the field induced phase transition will occur and the crystal will become rhombohedral (Wada et al., 1999). This is beyond the scope of this study.

Since all the three coexisting variants are pair-wise compatible with $\mathbf{n}_{ij}\|\langle 1\,1\,0\rangle$, we can construct such a three-variant system using a rank-two laminate as follows:

1. Choose variants 2 and 1 to construct a band $I$ with domain wall or interface normal given by $\mathbf{n}_{12}\|[1\,1\,0]$, and choose variants 2 and 3 to construct a band $J$ with domain wall given by $\mathbf{n}_{23}\|[0\,1\,1]$; in both bands the volume fraction of variant 2 is $\mu_1 = 1/3$.
2. Choose bands $I$ and $J$ to construct a rank-two laminate with interface normal given by $\mathbf{n}_{13}\|[1\,0\,1]$ and volume fraction of band $I$ given by $\mu_2 = 1/2$.

The construction is schematically shown in Fig. 3. Since the engineered domain configuration is a rank-two laminate, Eqs. (3.8) needs to be applied twice to determine the effective moduli of the single crystal. The effective moduli of bands $I$ and $J$ were calculated first using (3.8) with the electromechanical moduli of single-domain single crystal as input. Then the effective moduli of bands $I$ and $J$ were used as input to calculate the effective moduli of single crystal, which is then transformed into a new coordinate system with $x_1\|[\bar{1}\,2\,\bar{1}], x_2\|[\bar{1}\,0\,1], x_3\|[1\,1\,1]$ in order to be compared with experiments. When there is separation of scales between laminates, bands, and domains, so that bands $I$ and $J$ can be regarded as homogeneous as far as the macroscopic behavior

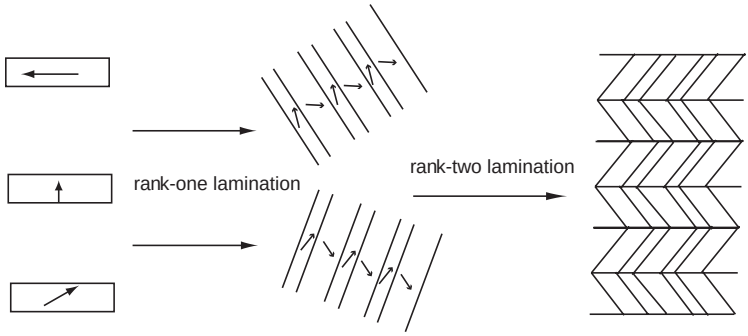


Fig. 3. The construction of energy minimizing domain configuration by rank-two laminate for tetragonal crystal poled along the [1 1 1] direction.

Table 1
Electromechanical moduli of single-domain single crystalline barium titanate, **S**: $10^{-12}$ $m^2/N$; **d**: $10^{-12}C/N$; $\kappa$: $\varepsilon_0$

| $S_{11}$ | $S_{12}$ | $S_{13}$ | $S_{33}$ | $S_{44}$ | $S_{66}$ | $d_{31}$ | $d_{33}$ | $d_{15}$ | $\kappa_{11}$ | $\kappa_{33}$ |
|---|---|---|---|---|---|---|---|---|---|---|
| 7.38 | −1.39 | −4.41 | 13.10 | 16.40 | 7.46 | −33.72 | 93.95 | 560.7 | 4367 | 132.5 |

of single crystal is concerned, the procedure leads to exact effective moduli of single crystal with engineered domain configuration. For barium titanate, the single-domain electroelastic moduli are listed in Table 1 (Zgonik et al., 1994). Using these data, we calculate the effective elastic, piezoelectric, and dielectric constants of barium titanate poled along the [1 1 1] axis as follows (**S** : $10^{-12}m^2/N$; **d** : $10^{-12}C/N$; $\kappa : \varepsilon_0$):

$$\mathbf{S} = \begin{bmatrix} 5.94 & -2.33 & -1.12 & 0 & 2.42 & 0 \\ -2.33 & 5.94 & -1.12 & 0 & -2.42 & 0 \\ -1.12 & -1.12 & 4.73 & 0 & 0 & 0 \\ 0 & 0 & 0 & 2.00 & 0 & -5.17 \\ 2.42 & -2.42 & 0 & 0 & 2.00 & 0 \\ 0 & 0 & 0 & -5.17 & 0 & 1.67 \end{bmatrix},$$

$$\mathbf{d} = \begin{bmatrix} -34.64 & 34.65 & 0 & 0 & 161.0 & 0 \\ 0 & 0 & 0 & 175.7 & 0 & 85.59 \\ -72.03 & -72.01 & 159.3 & 0 & 0 & 0 \end{bmatrix},$$

$$\kappa = \begin{bmatrix} 1055.0 & 0 & 0 \\ 0 & 954.22 & 0 \\ 0 & 0 & 2199.0 \end{bmatrix}.$$

From the calculations, we notice that the barium titanate poled along the [1 1 1] axis has symmetry very close to $3m$ (Nye, 1957). It is also confirmed that the three-variant domain configuration indeed leads to enhanced piezoelectricity, where piezoelectric coefficient $d_{33}$ is found to be 70% higher than that of single-domain single crystal, consistent with 62% enhancement observed in experiment (Wada et al., 1999). The single-domain piezoelectric coefficient $d_{33}$ was reported to be 125 pC/N in Wada et al. (1999), slightly higher than 93.95 pC/N reported by Zgonik et al. (1994). Most likely this is an extrinsic effect due to some 180° domain wall movement. In addition, piezoelectric coefficients $d_{31}$ and $d_{32}$ are about 114% higher than those of single-domain single crystal. As such, we are able to explain the enhanced piezoelectric coefficient observed in barium titanate poled along the [1 1 1] direction using the engineered domain configuration, which takes into account the energy minimizing domain configuration, the anisotropy of ferroelectric variants, and the interaction between ferroelectric domains. We not only demonstrate the enhancement in the longitudinal direction, which is consistent with experiment observation, but also predict the enhancement in the transverse direction which has yet to be reported in the literature. This is certainly worth investigating experimentally.

It is not clear, however, that if the barium titanate poled along the [1 1 1] axis is optimal as far as the electromechanical coupling is concerned. As such, we also consider a barium titanate poled by an electric field along the [0 1 1] axis combined with a compressive stress along the [1 0 0] axis, $\mathbf{E}_0 = [0, 1, 1]E_0$, $\mathbf{T}_0 = [-T_0, 0, 0]$. Under such electromechanical poling, variant 1 becomes energetically unfavored, leading to the coexistence of variants 2 and 3. Such a two-variant system can be constructed by a rank-one laminate with domain wall given by $\mathbf{n}_{23} = [0\,1\,1]$ and volume fraction given by $\mu = 1/2$. In a global coordinate system with $x_1 \| [1\,0\,0], x_2 \| [0\,1\,\bar{1}], x_3 \| [0\,1\,1]$, the effective elastic, piezoelectric, and dielectric constants for such barium titanate are calculated as follows, which possess $mm2$ symmetry:

$$\mathbf{S} = \begin{bmatrix} 7.38 & -2.90 & -2.90 & 0 & 0 & 0 \\ -2.90 & 7.02 & -1.18 & 0 & 0 & 0 \\ -2.90 & -1.18 & 7.02 & 0 & 0 & 0 \\ 0 & 0 & 0 & 26.31 & 0 & 0 \\ 0 & 0 & 0 & 0 & 10.26 & 0 \\ 0 & 0 & 0 & 0 & 0 & 11.93 \end{bmatrix},$$

$$\mathbf{d} = \begin{bmatrix} 0 & 0 & 0 & 0 & 248.0 & 0 \\ 0 & 0 & 0 & 137.2 & 0 & 0 \\ -23.85 & -176.9 & 219.5 & 0 & 0 & 0 \end{bmatrix},$$

$$\kappa = \begin{bmatrix} 2877.8 & 0 & 0 \\ 0 & 193.61 & 0 \\ 0 & 0 & 2249.5 \end{bmatrix}.$$

Table 2
Piezoelectric coefficients and electromechanical coupling factors of barium titanate crystals with engineered domain configuration; **d**: $10^{-12}$ C/N

| $d_{ij}$ | $d_{31}$ | $d_{32}$ | $d_{33}$ | $k_{31}$ (%) | $k_{32}$ (%) | $k_{33}$ (%) |
|---|---|---|---|---|---|---|
| Single crystal | −33.72 | −33.72 | 93.95 | 36 | 36 | 76 |
| Two-variant | −23.85 | −176.9 | 219.5 | 6 | 47 | 59 |
| Three-variant | −72.03 | −72.01 | 159.3 | 21 | 21 | 52 |

It is noted that for the two-variant system poled along the [0 1 1] direction, the piezoelectric coefficient $d_{32}$ is more than 400% higher than that of single-domain single crystal, and piezoelectric coefficient $d_{33}$ is more than 100% higher, suggesting much larger piezoelectric enhancement than the three-variant system. To our best knowledge, such two-variant engineered domain configuration has yet to be explored in experiment.

The predicted piezoelectric coefficients for both three- and two-variant crystals are summarized in Table 2. It is interesting to notice that although the piezoelectric coefficient $d_{33}$ is enhanced by the engineered domain configurations, the electromechanical coupling factor $k_{33}$ is actually reduced. On the other hand, barium titanate poled along [0 1 1] direction does have higher $k_{32}$ than that of single-domain crystal.

### 4.2. Rhombohedral crystal

We then consider rhombohedral crystals such as PMN–PT. The transformation strains and polarizations of rhombohedral ferroelectric are given by

$$\mathbf{e}^{(\pm1)} = \begin{bmatrix} \eta & \delta & \delta \\ \delta & \eta & \delta \\ \delta & \delta & \eta \end{bmatrix}, \quad \mathbf{p}^{(\pm1)} = \pm \begin{bmatrix} p_r \\ p_r \\ p_r \end{bmatrix},$$

$$\mathbf{e}^{(\pm2)} = \begin{bmatrix} \eta & -\delta & -\delta \\ -\delta & \eta & \delta \\ -\delta & \delta & \eta \end{bmatrix}, \quad \mathbf{p}^{(\pm2)} = \pm \begin{bmatrix} -p_r \\ p_r \\ p_r \end{bmatrix},$$

$$\mathbf{e}^{(\pm3)} = \begin{bmatrix} \eta & \delta & -\delta \\ \delta & \eta & -\delta \\ -\delta & -\delta & \eta \end{bmatrix}, \quad \mathbf{p}^{(\pm3)} = \pm \begin{bmatrix} -p_r \\ -p_r \\ p_r \end{bmatrix},$$

$$\mathbf{e}^{(\pm4)} = \begin{bmatrix} \eta & -\delta & \delta \\ -\delta & \eta & -\delta \\ \delta & -\delta & \eta \end{bmatrix}, \quad \mathbf{p}^{(\pm4)} = \pm \begin{bmatrix} p_r \\ -p_r \\ p_r \end{bmatrix}. \tag{4.2}$$

Table 3
Electromechanical moduli of PMN–PT, **S**: $10^{-12}$ $m^2/N$; **d**: $10^{-12}$ C/N; $\kappa$: $\varepsilon_0$

| $S_{11}$ | $S_{12}$ | $S_{13}$ | $S_{14}$ | $S_{33}$ | $S_{44}$ | $S_{66}$ |
|---|---|---|---|---|---|---|
| 62.16 | −53.85 | −5.58 | −166.24 | 13.34 | 510.98 | 232.02 |
| $d_{31}$ | $d_{33}$ | $d_{15}$ | $d_{22}$ | $\kappa_{11}$ | $\kappa_{33}$ | |
| −90 | 190 | 4100 | 1340 | 3950 | 640 | |

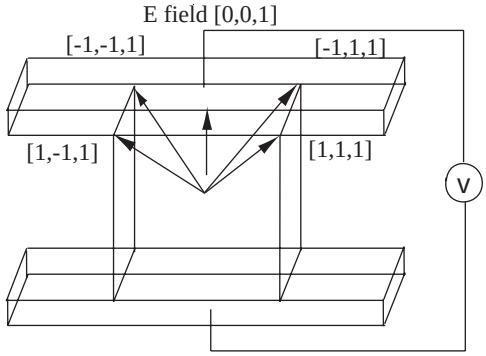


Fig. 4. The coexistence of four ferroelectric variants in the [0 0 1] poled rhombohedral crystal.

The total number of variants is 8. It can be easily verified that each pair of variants is compatible. The single-domain single crystal data of PMN–PT, which are used in the following calculations, are listed in Table 3 (Zhang et al., 2003a).

We first consider a rhombohedral crystal poled along the [0 0 1] axis, $\mathbf{E}_0 = [0, 0, E_0]$, with $\mathbf{T}_0 = \mathbf{0}$, as shown in Fig. 4. As a result of the poling, four variants with positive polarization component along $x_3$ axis will coexist in ferroelectric to minimize the potential energy with electric field. In addition, they will have equal volume fractions, $\lambda_i = 1/4$, to minimize the depolarization energy. Otherwise, the crystal will have net polarization components parallel to the (0 0 1) planes which are deposited with electrode, leading to nonzero depolarization field. Since the four variants are pair-wise compatible with $\mathbf{n}_{ij} \| \langle 1\,1\,0 \rangle$ or $\mathbf{n}_{ij} \| \langle 0\,0\,1 \rangle$, corresponding to 71° domain wall and 109° domain wall, we can construct such a four-variant system using a rank-three laminate as follows:

1. Construct bands $i$, $j$, $k$ using variant 1 with variants 2, 3, and 4, respectively, with domain wall or interface normals given by $\mathbf{n}_{12} \| [0\,1\,1]$, $\mathbf{n}_{13} \| [0\,0\,1]$, and $\mathbf{n}_{14} \| [1\,0\,1]$; the volume fraction of variant 1 is $\mu_1 = 1/4$ within each band.
2. Construct rank-two laminates $J$ and $K$ using band $i$ with bands $j$ and $k$, respectively, with interface normals given by $\mathbf{n}_{23} \| [\bar{1}\,0\,1]$ and $\mathbf{n}_{24} \| [0\,0\,1]$; the volume fraction of band $i$ within each laminate is $\mu_2 = 1/3$.

3. Construct a rank-three laminate using $J$ and $K$ with interface normal given by $\mathbf{n}_{34} \| [0\ \bar{1}\ 1]$ and volume fraction of band $I$ given by $\mu_3 = 1/2$.

Since the engineered domain configuration is a rank-three laminate, Eqs. (3.8) needs to be applied three times to determine the effective moduli of the single crystal. The calculated elastic, piezoelectric, and dielectric constants of PMN–PT, expressed in a coordinate system with $x_1 \| [1\,0\,0]$, $x_2 \| [0\,1\,0]$, $x_3 \| [0\,0\,1]$ in order to be compared with experiments, are given as follows, which has symmetry very close to $4m$:

$$\mathbf{S} = \begin{bmatrix} 240.3 & -121.0 & -116.8 & 0 & 0 & 0 \\ -121.0 & 240.6 & -117.0 & 0 & 0 & 0 \\ -116.8 & -117.0 & 236.3 & 0 & 0 & 0 \\ 0 & 0 & 0 & 14.7 & 0 & 0 \\ 0 & 0 & 0 & 0 & 15.3 & 0 \\ 0 & 0 & 0 & 0 & 0 & 16.5 \end{bmatrix},$$

$$\mathbf{d} = \begin{bmatrix} 0 & 0 & 0 & 0 & 70.0 & 0 \\ 0 & 0 & 0 & 63.5 & 0 & 0 \\ -1099.4 & -1102.0 & 2207.2 & 0 & 0 & 0 \end{bmatrix},$$

$$\kappa = \begin{bmatrix} 311.5 & 0 & 0 \\ 0 & 303.1 & 0 \\ 0 & 0 & 2705.3 \end{bmatrix}.$$

The rank-three laminate follows from a general procedure for constructing the energy-minimizing microstructure with $N$ pair-wise compatible variants. A detailed examination of four variants available here, however, suggests that simpler rank-two laminates are also possible. For example, we can use variants 1 and 3 with equal volume fractions to construct a band $I$ of orthorhombic symmetry,

$$\mathbf{e}^I = \begin{bmatrix} \eta & \delta & 0 \\ \delta & \eta & 0 \\ 0 & 0 & \eta \end{bmatrix}, \quad \mathbf{p}^I = \begin{bmatrix} 0 \\ 0 \\ p \end{bmatrix}.$$

Similarly, we can construct a band $J$ using variants 2 and 4,

$$\mathbf{e}^J = \begin{bmatrix} \eta & -\delta & 0 \\ -\delta & \eta & 0 \\ 0 & 0 & \eta \end{bmatrix}, \quad \mathbf{p}^J = \begin{bmatrix} 0 \\ 0 \\ p \end{bmatrix}.$$

In each band, only 109° domain walls exist. Clearly, bands $I$ and $J$ have effective orthorhombic symmetry, and are compatible with each other with interface normal given by [0 1 0] (Shu and Bhattacharya, 2001). Thus they can form another level of laminate to represent crystals poled along the [0 0 1] direction. The calculated elastic, piezoelectric, and dielectric constants of PMN–PT are given as follows, which has symmetry very close to $4m$:

$$\mathbf{S} = \begin{bmatrix} 244.7 & -121.1 & -121.1 & 0 & 0 & 0 \\ -121.1 & 244.7 & -121.1 & 0 & 0 & 0 \\ -121.1 & -121.1 & 244.7 & 0 & 0 & 0 \\ 0 & 0 & 0 & 13.2 & 0 & 0 \\ 0 & 0 & 0 & 0 & 13.8 & 0 \\ 0 & 0 & 0 & 0 & 0 & 20.0 \end{bmatrix},$$

$$\mathbf{d} = \begin{bmatrix} 0 & 0 & 0 & 0 & 51.2 & 0 \\ 0 & 0 & 0 & 50.4 & 0 & 0 \\ -1151.8 & -1151.8 & 2309.4 & 0 & 0 & 0 \end{bmatrix},$$

$$\kappa = \begin{bmatrix} 282.9 & 0 & 0 \\ 0 & 287.2 & 0 \\ 0 & 0 & 2846.7 \end{bmatrix}.$$

In a similar manner, bands $I$ and $J$ can also be constructed to contain only 71° domain walls using variants 1 and 4, and variants 2 and 3, respectively, so that

$$\mathbf{e}^I = \begin{bmatrix} \eta & 0 & \delta \\ 0 & \eta & 0 \\ \delta & 0 & \eta \end{bmatrix}, \quad \mathbf{p}^I = \begin{bmatrix} p \\ 0 \\ p \end{bmatrix},$$

and

$$\mathbf{e}^J = \begin{bmatrix} \eta & 0 & -\delta \\ 0 & \eta & 0 \\ -\delta & 0 & \eta \end{bmatrix}, \quad \mathbf{p}^J = \begin{bmatrix} -p \\ 0 \\ p \end{bmatrix}.$$

They are again compatible with each other and have orthorhombic symmetry. In this case, the interface normal between bands $I$ and $J$ is [0 0 1]. The calculated elastic, piezoelectric, and dielectric constants are given as follows, which possesses

$2mm$ symmetry,

$$\mathbf{S} = \begin{bmatrix} 235.4 & -121.1 & -111.8 & 0 & 0 & 0 \\ -121.1 & 244.7 & -121.1 & 0 & 0 & 0 \\ -111.8 & -121.1 & 235.4 & 0 & 0 & 0 \\ 0 & 0 & 0 & 14.1 & 0 & 0 \\ 0 & 0 & 0 & 0 & 16.1 & 0 \\ 0 & 0 & 0 & 0 & 0 & 14.9 \end{bmatrix},$$

$$\mathbf{d} = \begin{bmatrix} 0 & 0 & 0 & 0 & 85.9 & 0 \\ 0 & 0 & 0 & 49.2 & 0 & 0 \\ -1038.5 & -1151.8 & 2196.1 & 0 & 0 & 0 \end{bmatrix},$$

$$\kappa = \begin{bmatrix} 337.0 & 0 & 0 \\ 0 & 280.5 & 0 \\ 0 & 0 & 2690.0 \end{bmatrix}.$$

Since there are less interfaces involved in rank-two laminates, they are more likely to occur in crystals. Indeed, interweaving domain configurations containing either 109° or 71° domain walls have been observed in PMN–PT crystals poled along [0 0 1] directions (Zhang et al., 2003b). The calculated piezoelectric coefficients $d_{31}$ and $d_{33}$ and electromechanical coupling factors $k_{31}$ and $k_{33}$ of four-variant PMN–PT with various kinds of engineered domain configurations are summarized in Table 4, and compared with measured values for PMN–PT poled along the [0 0 1] axis (Zhang et al., 2001). It is observed that the effective piezoelectric coefficients and electromechanical coupling factors calculated using rank-three and rank-two laminates agree well with experiment measurement, especially for the electromechanical coupling factor $k_{33}$, which shows excellent agreement with experiment. Among all three domain configurations, the rank-two laminate with 109° domain wall agrees with measurement best. This suggests that the enhanced piezoelectricity is indeed related to the engineered domain configurations.

Table 4
Elastic constant, piezoelectric constants, dielectric constants and electromechanical coupling factors of single crystalline PMN–PT poled along the [0 0 1] direction; **d**: $10^{-12}$ C/N; $\kappa$: $\varepsilon_0$

| | $d_{31}$ | $d_{33}$ | $k_{31}$ (%) | $k_{33}$ (%) |
|---|---|---|---|---|
| Rank-3 | −1099.4 | 2207.2 | 46 | 93 |
| Rank-2 (109°) | −1151.8 | 2309.4 | 46 | 93 |
| Rank-2 (71°) | −1038.5 | 2196.1 | 44 | 93 |
| Experiment | −1330 | 2820 | 59 | 94 |

It remains to be seen, again, that if the PMN-PT poled along the [0 0 1] axis is optimal as far as the electromechanical couplings is concerned. In particular, there is only a modest increase in $k_{31}$ for this four-variant system. As such, we also consider a PMN–PT crystal poled by an electric field along the [0 0 1] direction, $\mathbf{E}_0 = [0, 0, 1]E_0$, combined with a positive shear stress $\sigma_{12}$ applied at the boundary. Due to the applied shear stress, variants 2 and 4 become energetically unfavored, leading to the coexistence of variants 1 and 3 by 109° domain wall, $\mathbf{n}_{13} = [0\,0\,1]$. The domain configuration can be constructed by a rank-one laminate which requires the application of (3.8) only once. The elastic, piezoelectric, and dielectric constants of this PMN–PT are calculated as following:

$$\mathbf{S} = \begin{bmatrix} 62.2 & 56.7 & -116.1 & 0 & 0 & 0 \\ 56.7 & 71.7 & -126.0 & 0 & 0 & 0 \\ -116.1 & -126.0 & 244.7 & 0 & 0 & 0 \\ 0 & 0 & 0 & 16.7 & 0 & 0 \\ 0 & 0 & 0 & 0 & 11.0 & 0 \\ 0 & 0 & 0 & 0 & 0 & 731.5 \end{bmatrix},$$

$$\mathbf{d} = \begin{bmatrix} 0 & 0 & 0 & 0 & 40.6 & 0 \\ 0 & 0 & 0 & 65.3 & 0 & 0 \\ -1146.1 & -1157.6 & 2309.4 & 0 & 0 & 0 \end{bmatrix},$$

$$\kappa = \begin{bmatrix} 248.6 & 0 & 0 \\ 0 & 328.2 & 0 \\ 0 & 0 & 2846.7 \end{bmatrix}.$$

Similarly, we can pole the PMN–PT crystal by an electric field along the [0 1 1] axis, $\mathbf{E}_0 = [0, 1, 1]E_0$, which disfavors variants 3 and 4, leading to the coexistence of variants 1 and 2 by 71° domain wall, $\mathbf{n}_{12} = [0\,1\,1]$. In such case, the final coordinate system is chosen to be $x_1 \| [0\,\bar{1}\,1]$, $x_2 \| [1\,0\,0]$, and $x_3 \| [0\,1\,1]$, so that $x_3$ is parallel to the poling direction. The elastic, piezoelectric, and dielectric constants of the [0 1 1] poled PMN–PT are calculated as following:

$$\mathbf{S} = \begin{bmatrix} 62.2 & -116.1 & 56.7 & 0 & 0 & 0 \\ -116.1 & 244.7 & -126.0 & 0 & 0 & 0 \\ 56.7 & -126.0 & 71.7 & 0 & 0 & 0 \\ 0 & 0 & 0 & 18.2 & 0 & 0 \\ 0 & 0 & 0 & 0 & 694.4 & 0 \\ 0 & 0 & 0 & 0 & 0 & 11.5 \end{bmatrix},$$

Table 5
Piezoelectric coefficients and electromechanical coupling factors of two-variant single crystal, poled along [0 0 1] or ⟨0 1 1⟩ directions; **d**: $10^{-12}$ C/N; $\kappa$: $\varepsilon_0$

| | $d_{31}$ | $d_{32}$ | $d_{33}$ | $k_{31}$ (%) | $k_{32}$ (%) | $k_{33}$ (%) |
|---|---|---|---|---|---|---|
| Two-variant ([0 0 1] poling + $\sigma_{12}$) | −1146.1 | −1157.6 | 2309.4 | 92 | 86 | 93 |
| Two-variant (⟨0 1 1⟩ poling) | 700.2 | −1628.9 | 936.9 | 71 | 84 | 89 |
| Experiment (⟨0 1 1⟩ poling) | 690 | −1670 | 980 | | | |

$$\mathbf{d} = \begin{bmatrix} 0 & 0 & 0 & 0 & 4574.4 & 0 \\ 0 & 0 & 0 & 89.8 & 0 & 0 \\ 700.2 & -1628.9 & 936.9 & 0 & 0 & 0 \end{bmatrix},$$

$$\kappa = \begin{bmatrix} 3636.6 & 0 & 0 \\ 0 & 311.1 & 0 \\ 0 & 0 & 1743.3 \end{bmatrix}.$$

The calculations, along with measured piezoelectric coefficients of a similar crystal PZN–PT poled along the [1 1 0] axis (Liu and Lynch, 2003), are summarized in Table 5. Again, we observed excellent agreement between our calculation and experimental measurement for crystal poled along the ⟨1 1 0⟩ direction. In addition, crystal electromechanically poled along the [0 0 1] direction with two variants coexisting has superior electromechanical coupling coefficients $k_{31}$, $k_{32}$, and $k_{33}$ simultaneously. $k_{33}$ is comparable to that of four-variant system, while $k_{31}$ is much higher. This suggests that the two-variant system poled along the [0 0 1] direction with appropriate shear stress applied is optimal for electromechanical coupling. Such new poling procedure is certainly worthy investigation experimentally.

## 5. Concluding remarks

In summary, we have characterized the engineered domain configurations in ferroelectric crystals using energy minimizing multi-rank lamination. The effective electromechanical properties of ferroelectric crystals with engineered domain configurations have been calculated and good agreement with experimental measurements has been observed. We are also able to identify the optimal domain configurations and poling directions for the enhanced electromechanical coupling.

## Acknowledgements

We are deeply grateful to Kaushik Bhattacharya for his continuous encouragement and numerous discussions, and for comments on the draft. We are glad to acknowledge

the financial support from National Science Foundation (CMS-0415261), Nebraska EPSCoR, and University of Nebraska-Lincoln.

## References

Ball, J.M., James, R.D., 1992. Proposed experimental tests of a theory of fine microstructure and the two well problem. Philos. Trans. Roy. Soc. London A 338, 389–450.

Bellaiche, L., Garcia, A., Vanderbilt, D., 2000. Finite-temperature properties of $Pb(Zr_{1-x}Ti_x)O_3$ alloys from first principles. Phys. Rev. Lett. 84, 5427–5430.

Bhattacharya, K., 1993. Comparison of geometrically nonlinear and linear theories of martensitic-transformation. Continuum Mech. Therm. 5, 205–242.

Bhattacharya, K., Ravichandran, G., 2003. Ferroelectric perovskites for electromechanical actuation. Acta Mater. 51, 5941–5960.

Brown, W.F., 1963. Micromagnetics. Interscience Publishers, New York.

Chen, X., Fang, D.N., Hwang, K.C., 1997. Micromechanics simulation of ferroelectric polarization switching. Acta Mater. 45, 3181–3189.

DeSimone, A., 1993. Energy minimizers for large ferromagnetic bodies. Arch. Rat. Mech. Anal. 125, 99–143.

DeSimone, A., James, R.D., 2002. A constrained theory of magnetoelasticity. J. Mech. Phys. Solids 50, 283–320.

Dunn, M.L., 1995. Effects of grain shape anisotropy, porosity, and microcracks on the elastic and dielectric constants of polycrystalline piezoelectric ceramics. J. Appl. Phys. 78, 1533–1542.

Fu, H.X., Cohen, R.E., 2000. Polarization rotation mechanism for ultrahigh electromechanical response in single-crystal piezoelectrics. Nature 403, 281–283.

Hu, H.L., Chen, L.Q., 1998. Three-dimensional computer simulation of ferroelectric domain formation. J. Am. Ceram. Soc. 81, 492–500.

Huber, J.E., Fleck, N.A., Landis, C.M., McMeeking, R.M., 1999. A constitutive model for ferroelectric polycrystals. J. Mech. Phys. Solids 47, 1663–1697.

Hwang, S.C., Lynch, C.S., McMeeking, R.M., 1995. Ferroelectric/ferroelastic interactions and a polarization switching model. Acta Metall. Mater. 43, 2073–2084.

James, R.D., Kinderlehrer, D., 1993. Theory of magnetostriction with applications to $Tb_xDy_{1-x}Fe_2$. Philos. Mag. 68, 237–274.

Jona, F., Shirane, G., 1993. Ferroelectric Crystals. Dover Publications, New York.

Kuwata, J., Uchino, K., Nomura, S., 1982. Dielectric and piezoelectric properties of $0.91Pb(Zn_{1/3}Nb_{2/3})O_3$–$0.09PbTiO_3$ single crystals. Jpn. J. Appl. Phys. 21, 1298–1302.

Li, J.Y., 2000. The effective electroelastic moduli of textured piezoelectric polycrystalline aggregates. J. Mech. Phys. Solids 48, 529–552.

Li, J., Weng, G.J., 1999. A Theory of domain switching for the nonlinear behavior of ferroelectrics. Proc. Roy. Soc. London A 455, 3493–3511.

Li, Y.L., Hu, S.Y., Liu, Z.K., Chen, L.Q., 2001. Phase-field model of domain structures in ferroelectric thin films. Appl. Phys. Lett. 78, 3878–3880.

Liu, D., Li, J.Y., 2003. The enhanced and optimal piezoelectric coefficients in single crystalline barium titanate with engineered domain configurations. Appl. Phys. Lett. 83 (6), 1193–1195.

Liu, T., Lynch, C.S., 2003. Ferroelectric properties of [1 1 0], [0 0 1] and [1 1 1] poled relaxor single crystals: measurements and modeling. Acta Mater. 51, 407–417.

Milton, G.W., 2002. The Theory of Composites. Cambridge University Press, Cambridge, UK.

Nambu, S., Sagala, D.A., 1994. Domain formation and elastic long-range interaction in ferroelectric perovskites. Phys. Rev. B 50, 5838–5847.

Nye, J.F., 1957. Physical Properties of Crystals. Oxford University Press, Oxford, UK.

Park, S.E., Shrout, T.R., 1997. Ultrahigh strain and piezoelectric behavior in relaxor based ferroelectric single crystals. J. Appl. Phys. 82, 1804–1811.

Park, S.E., Wada, S., Cross, L.E., Shrout, T.R., 1999. Crystallographically engineered $BaTiO_3$ single crystals for high-performance piezoelectrics. J. Appl. Phys. 86, 2746–2750.

Shu, Y.C., Bhattacharya, K., 2001. Domain patterns and macroscopic behaviour of ferroelectric materials. Philos. Mag. B 81, 2021–2054.

Wada, S., Suzuki, S., Noma, T., Suzuki, T., Osada, M., Kakihana, M., Park, S.E., Cross, L.E., Shrout, T.R., 1999. Enhanced piezoelectric property of barium titanate single crystals with engineered domain configurations. Jpn. J. Appl. Phys. 38, 5505–5511.

Zgonik, M., Bernasconi, P., Duelli, M., chlesser, R., Gunter, P., Garrett, M.H., Rytz, D., Zhu, Y., Wu, X., 1994. Dielectric, elastic, piezoelectric, electrooptic, and elasto-optic tensors of $BaTiO_3$ crystals. Phys. Rev. B 50, 5941–5950.

Zhang, R., Jiang, B., Cao, W.W., 2001. Elastic, piezoelectric, and dielectric properties of multidomain $0.67Pb(Mg_{1/3}Nb_{2/3})O_3$–$0.33PbTiO_3$ single crystals. J. Appl. Phys. 90, 3471–3475.

Zhang, R., Jiang, B., Cao, W.W., 2003a. Single-domain properties of $0.67Pb(Mg_{1/3}Nb_{2/3})O_3$–$0.33PbTiO_3$ single crystals under electric field bias. Appl. Phys. Lett. 82, 787–789.

Zhang, R., Jiang, B., Cao, W.W., 2003b. Interweaving domain configurations in [0 0 1]-poled rhombohedral phase $0.67Pb(Mg_{1/3}Nb_{2/3})O_3$–$0.33PbTiO_3$ single crystals. Appl. Phys. Lett. 83, 2040–2042.